


APRIL 08 2024

# High-speed and acceleration micrometric jets induced by GHz streaming: A numerical study with direct numerical simulations

Virginie Daru  ; Bjarne Vincent  ; Michael Baudoin 

 Check for updates

*J. Acoust. Soc. Am.* 155, 2470–2481 (2024)

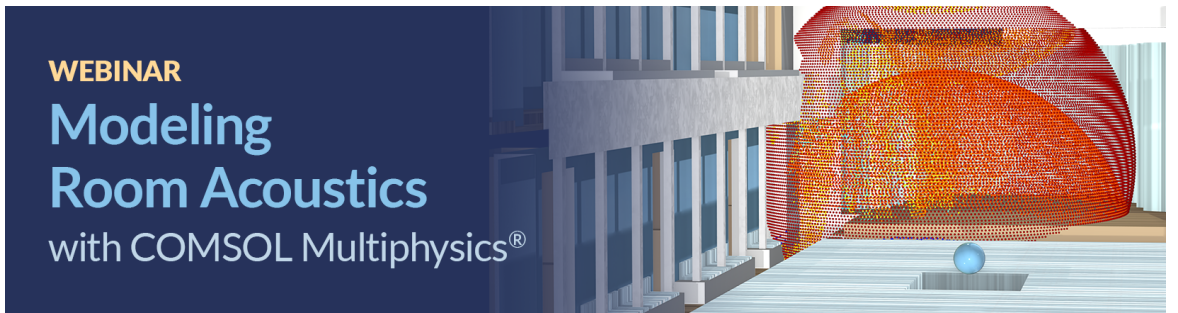
<https://doi.org/10.1121/10.0025462>






WEBINAR

## Modeling Room Acoustics

with COMSOL Multiphysics®



## High-speed and acceleration micrometric jets induced by GHz streaming: A numerical study with direct numerical simulations

Virginie Daru,<sup>1,a)</sup>  Bjarne Vincent,<sup>2,3</sup>  and Michael Baudoin<sup>4,5,b)</sup> 

<sup>1</sup>*DynFluid Lab, Arts & Métiers Science & Technology, 151 boulevard de l'hôpital, 75013, Paris, France*

<sup>2</sup>*Institut National des Sciences Appliquées Lyon, CNRS, Ecole Centrale de Lyon, Université Claude Bernard Lyon 1, Laboratoire de Mécanique des Fluides et d'Acoustique, Unité Mixte de Recherche 5509, 69621, Villeurbanne, France*

<sup>3</sup>*Fluid and Complex Systems Research Centre, Coventry University, Coventry CV15FB, United Kingdom*

<sup>4</sup>*Université Lille, CNRS, Centrale Lille, Université Polytechnique Hauts-de-France, Unité Mixte de Recherche 8520, Institut d'Electronique, de Microélectronique et de Nanotechnologie, F59000 Lille, France*

<sup>5</sup>*Institut Universitaire de France, 1 rue Descartes, 75005, Paris, France*

### ABSTRACT:

Gigahertz acoustic streaming enables the synthesis of localized microjets reaching speeds of up to meters per second, offering tremendous potential for precision micromanipulation. However, theoretical and numerical investigations of acoustic streaming at these frequencies remain so far relatively scarce due to significant challenges including: (i) the inappropriateness of classical approaches, rooted in asymptotic development, for addressing high-speed streaming with flow velocities comparable to the acoustic velocity; and (ii) the numerical cost of direct numerical simulations generally considered as prohibitive. In this paper, we investigate high-frequency bulk streaming using high-order finite difference direct numerical simulations. First, we demonstrate that high-speed micrometric jets of several meters per second can only be obtained at high frequencies, due to diffraction limits. Second, we establish that the maximum jet streaming speed at a given actuation power scales with the frequency to the power of  $3/2$  in the low attenuation limit and linearly with the frequency for strongly attenuated waves. Last, our analysis of transient regimes reveals a dramatic reduction in the time required to reach the maximum velocity as the frequency increases (power law in  $-5/2$ ), leading to characteristic time on the order of  $\mu\text{s}$  at gigahertz frequencies, and hence accelerations within the Mega-g range. © 2024 Acoustical Society of America. <https://doi.org/10.1121/10.0025462>

(Received 12 October 2023; revised 11 February 2024; accepted 11 March 2024; published online 8 April 2024)

[Editor: Likun Zhang]

Pages: 2470–2481

### I. INTRODUCTION

Gigahertz (GHz) streaming is receiving increasing interest, thanks to the emergence of mature advanced technologies for generating acoustic waves at these frequencies and the myriad possibilities offered by high-speed micrometric jets for fluid and particle manipulation (Wei *et al.*, 2023).

Acoustic waves in the GHz range can be generated using various techniques, including surface acoustic waves (SAWs), lamb wave (LWs) or bulk wave (BW) resonators. High-frequency SAWs can be synthesized on the surface of piezoelectric crystals using miniaturized interdigital transducers (IDTs) (Yeo and Friend, 2014). In this case, acoustic energy remains localized at the substrate's surface, so that the use of thin films is not required. Shilton *et al.* (2014) demonstrated fluid actuation at GHz frequencies using SAWs to achieve mixing in nanoliter droplets. In the same year, Dentry *et al.* (2014) studied streaming jets generated by SAWs for frequencies up to 936 MHz. Additionally, Collins *et al.* (2016b) reported highly localized acoustic

streaming vortices in microchannels generated by focused IDTs at frequencies approaching the GHz range (636 MHz).

Generating high-frequency LWs requires more advanced technologies due to the following factors: (i) The thickness of the piezoelectric layer used for wave synthesis must be on the order of or smaller than the wavelength to generate flexural or extensional modes, necessitating the use of thin films. (ii) To prevent the transmission of wave energy, the transducer must be isolated from its support. Consequently, high-frequency LWs are typically synthesized using LW contour mode resonators, comprising a thin suspended piezoelectric film actuated with IDTs. High-frequency contour mode resonators have been introduced in the field of acoustofluidics by Duan *et al.* (Liu *et al.*, 2018; Zhang *et al.*, 2018). However, while they can operate in the GHz range (Zuo *et al.*, 2009), their possibilities have not been explored so far in this regime for fluid actuation.

Finally, GHz BW resonators are created by exciting longitudinal bulk modes in piezoelectric thin films sandwiched between two electrodes. To minimize losses in the supporting substrate, these resonators can either be suspended, as in the thin-film bulk acoustic wave resonator (Lakin, 2003), implemented on a Bragg reflector to form

<sup>a)</sup>Email: virginie.daru@ensam.eu

<sup>b)</sup>Email: michael.baudoin@univ-lille.fr

solid mounted resonators (Lakin *et al.*, 1995), or deposited on the underside of a thicker substrate, which serves as a propagation medium and on top of which the microfluidics setup is attached (Ravi *et al.*, 2018). It is worth noting that, in the latter case, focused waves have been generated at GHz frequencies using Fresnel-type patterned electrodes, similar to the principle employed by Riaud *et al.* (2017a) and Baudoin *et al.* (2019) for synthesizing acoustical vortices.

With these BW GHz setups, high-speed jets reaching velocities of several meters per second, comparable to the acoustic velocity, have been reported (Eisener *et al.*, 2015; Wu *et al.*, 2022). These high-speed jets have been effectively utilized for various fluid manipulation tasks, including mixing (Cui *et al.*, 2016; Ravi *et al.*, 2018), droplet dispensing (He *et al.*, 2018), and concentration as well as manipulation of micro- and nano-particles (Cui *et al.*, 2018, 2019; Guo *et al.*, 2020; Shi *et al.*, 2022; Yang *et al.*, 2022) within microfluidic setups. It is important to note that, in contrast to classical miniaturized tweezers based on standing waves (Ding *et al.*, 2012; Tran *et al.*, 2012), acoustic vortices (Baudoin *et al.*, 2019, 2020; Riaud *et al.*, 2017a; Sahely *et al.*, 2022), or pulsed methods (Chen *et al.*, 2023; Collins *et al.*, 2016a; Kim *et al.*, 2023; Wang *et al.*, 2021), which rely on the acoustic radiation force, manipulation in this case is accomplished using the Stokes drag induced by the jet (Wei *et al.*, 2023). The unique capabilities offered by these GHz acoustic manipulation techniques have paved the way for a new set of applications in biology, including controlled loading and release of vesicles (Lu *et al.*, 2019), modulation of neurite outgrowth (He *et al.*, 2021), and the manipulation of carbon dots to enhance bioimaging and biosensing (Zhang *et al.*, 2022).

However, from a theoretical perspective, modeling high-speed acoustic streaming at GHz frequencies remains a challenging task because the streaming speed can be of the same order as the acoustic speed, rendering classical approaches based on asymptotic developments invalid (Baudoin and Thomas, 2020). For instance, Duan *et al.* (Wu *et al.*, 2022) employed a steady-state vs harmonic decomposition approach, which, nevertheless, assumes that the steady-state components are much smaller than the harmonic components and is only suited for describing steady streaming. Steckel and Bruus (2020) modeled the entire problem of GHz streaming synthesis with AlN thin films, but only within the low-speed limit.

Since the early discussions by Stuart (1963) and Lighthill (1978), there have been nevertheless various attempts to address the low-speed limitation of streaming modeling. Gusev and Rudenko (1979) investigated quasi-one dimensional streaming, considering hydrodynamic nonlinearities. Subsequently, Moudjed *et al.* (2014) employed a time-scale discrimination approach, which segregates the field between fluctuating and time-averaged fields, reminiscent of the decomposition used in turbulence modeling. Using this approach, they derived scaling laws for the characteristic velocity of streaming jets as a function of applied

power. Notably, Baudoin and Thomas (2020) and Riaud *et al.* (2017b) adopted a similar approach to develop a unified model that encompasses nonlinear wave propagation, acoustic streaming, and radiation pressure, providing a simple expression for the Eckart Streaming source term. However, these authors simplified the acoustic streaming source term in the low-speed limit. More recently, Orosco and Friend (2022) proposed an original approach involving both time and spatial scale separation. Nevertheless, most of these works (i) are confined to relatively ideal configurations, (ii) lack comparison to direct numerical simulations or precise characterization of experimental velocity profiles, and (iii) have not been applied in the GHz range.

From a numerical perspective, the cost of direct numerical simulation of bulk acoustic streaming is generally considered prohibitive; and to the best of our knowledge, no such simulations have been reported in the literature so far.

In this paper, we employ a high-order finite difference code to perform direct numerical simulations of the Navier-Stokes compressible equations and compute transient and steady acoustic streaming. The simulations cover a wide range of parameters, including various transducer apertures and frequencies. First, these simulations reveal that high-speed micrometric jets of several meters per second can only be achieved at high frequencies due to diffraction limitations. Second, the numerical simulations indicate the scaling of jet speed with frequency transitions from a 3/2 power law to a linear power law as the attenuation length becomes comparable to the Fresnel length, a trend rationalized with scaling analysis. Finally, we leverage the unique opportunity presented by direct numerical simulations to investigate the transient development of acoustic streaming. This transient analysis demonstrates that, at GHz frequencies, maximum velocities of up to tens of meters per second are reached in just a few microseconds, resulting in tremendous accelerations on the order of  $10^6$  g (Mega-g). The physical insights provided by these numerical simulations establish a solid foundation for the development of appropriate theories for high-frequency streaming.

## II. NUMERICAL METHOD

The configuration studied here is represented in Fig. 1. A plane acoustic wave of limited aperture is generated by a cylindrical vibrating piston inside a liquid (water) initially at rest in a cylinder. The right end of the cylinder is open such that the flow is free to exit, while the lateral wall and the wall surrounding the piston are considered as solid walls.

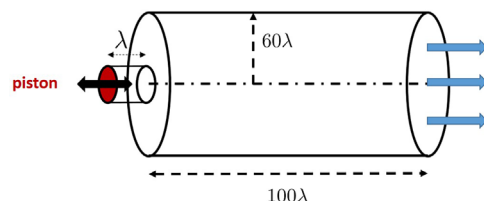


FIG. 1. (Color online) Sketch of the geometry of the simulated problem. The piston has a radius equal to  $R_p$ .

To perform simulations over a large range of frequencies, the dimensions of the simulation box (cylinder) are taken proportional to the wavelength and both the radius ( $R_{cyl} = 60\lambda$ ) and length of the simulation box ( $L_{cyl} = 100\lambda$ ) are chosen to be much larger than the acoustic source radius ( $R_p$ ) to avoid interference of the radiated wave and jet with the walls. We consider piston radii  $R_p$  between  $0.5\lambda$  and  $8\lambda$  and a wide frequency range varying from 37.5 MHz to 3 GHz. This upper limit of 3 GHz is chosen for our numerical investigation, as it corresponds to the maximum frequency reported in the literature for experimental investigations of acoustic streaming. In all calculations, the injected power  $P_{source}$  is kept constant, leading to a piston displacement amplitude proportional to  $R_p/\lambda$ , since the power is proportional to  $(v_p R_p)^2$ ,  $v_p$  being the piston velocity amplitude. The absolute value of  $P_{source}$  was chosen to reach streaming velocity on the order of meters per second in the GHz range in agreement with experiments (Eisener *et al.*, 2015).

The numerical approach consists of finite difference direct numerical solution of the isentropic compressible Navier-Stokes equations written in axisymmetric formulation:

$$\begin{cases} \frac{\partial \rho}{\partial t} + \nabla \cdot (\rho \mathbf{v}) = 0, \\ \frac{\partial (\rho \mathbf{v})}{\partial t} + \nabla \cdot (\rho \mathbf{v} \otimes \mathbf{v}) + \nabla p = \nabla \cdot \bar{\bar{\tau}}, \end{cases} \quad (1)$$

with  $\rho$  is the density,  $\mathbf{v} = (v_r, v_z)$  the velocity,  $p$  the pressure, and  $\bar{\bar{\tau}}$  the viscous tensor. The bulk viscosity  $\mu_B$  is taken into account, such that  $\bar{\bar{\tau}} = 2\mu\bar{\bar{D}} + (\mu_B - \frac{2}{3}\mu)\nabla \cdot \mathbf{v}\bar{\bar{I}}$ , where  $\mu$  is the shear viscosity,  $\bar{\bar{D}} = \bar{\bar{\nabla}}^s \mathbf{v}$  the strain tensor, with  $\bar{\bar{\nabla}}^s \mathbf{v}$  the symmetric part of the velocity gradient tensor. Pressure and density are related by an isentropic equation of state of first order:  $p - p_0 = c_0^2(\rho - \rho_0)$ , with  $c_0$  the speed of sound, the variables indexed 0 being the initial values. For water, the following values are used:  $\rho_0 = 1000 \text{ kg m}^{-3}$ ,  $c_0 = 1500 \text{ m s}^{-1}$ ,  $\mu = 10^{-3} \text{ kg m}^{-1} \text{ s}^{-1}$ ,  $\mu_B = 2.4 \times 10^{-3} \text{ kg m}^{-1} \text{ s}^{-1}$ . The system is operated at standard atmospheric pressure  $p_0 = 101325 \text{ Pa}$ . A no slip Dirichlet boundary condition  $\mathbf{v} = 0$  is applied on the lateral wall of the cylinder and around the piston. The vibration of the piston is simulated by applying an arbitrary Lagrangian-Eulerian method (Hirt *et al.*, 1974) to the grid portion surrounding the piston, and the corresponding grid portion is moving and deformable. The free flow in the outlet is simulated with a nonreflecting boundary condition that is well approximated by a Neuman condition in our case (nearly plane wave). Note that owing to this free flow condition and the large radius of the simulation box compared to the size of the piston, the interaction of both the acoustic wave and streaming flow with the lateral and right boundaries is negligible.

System (1) is solved using an explicit high-order finite difference scheme that was developed in Daru and Tenaud (2004) for inviscid compressible flows, and later extended for viscous flows (e.g., Daru and Tenaud, 2009). It uses upwind formulae of order 7 for the convective terms, and

centered formulae of order 2 for the viscous terms. The scheme is based on a coupled time and space (one-step) approach, resulting in the same formal order of accuracy in time and space for the convective part. The grid is Cartesian, uniform across the radius of the piston, stretched in the radial direction above, and uniform in the axial direction. The acoustic wavelength is discretized using 20 grid points per wavelength, that was proven to provide a sufficient accuracy for a good representation of the acoustic wave (Daru and Gloerfelt, 2007). The scheme being explicit, the time step  $\delta t$  is limited by the stability condition:  $(\delta t / \delta x)c_0 = \text{CFL}$  (Courant-Friedrich-Levy)  $\leq 1$ ,  $\delta x$  being the size of the smallest cell. This gives  $T / \delta t = (1/\text{CFL})\lambda / \delta x$ , where  $T = 1/f$  is the time period. In our calculations, we fixed  $\text{CFL} = 0.5$ , such that 40 time iterations per time period were necessary. This results in a large number of iterations (several hundreds of thousands of time steps) to reach steady streaming. Indeed, while the acoustic wave is very rapidly established in the domain, the streaming flow takes a much longer time to reach a steady state. Since direct numerical simulations are performed, the acoustic and streaming contributions are not naturally separated. To differentiate them and analyze the results, all variables  $\phi$  are hence subsequently decomposed into average and fluctuating values,  $\phi = \bar{\phi} + \phi'$ , such that the average value (corresponding to the streaming terms) is calculated from a simple arithmetic average over an acoustic time period of the variables,  $\bar{\phi} = 1/T \int_t^{t+T} \phi(t) dt$ , and the fluctuations (corresponding to the acoustic contribution) are simply obtained by subtracting the average field from the total field,  $\phi' = \phi - \bar{\phi}$ . Note that since the field is averaged over a single period, this definition is perfectly compatible with the study of unsteady streaming.

### III. DIFFRACTION-INDUCED LIMITATIONS FOR THE SYNTHESIS OF MICROJETS

#### A. Problem statement

A natural idea to synthesize micrometric jets with high speed would be to concentrate the emitted power on a source of reduced (micrometric) dimension. In this section, we study how the streaming evolves as the radial dimension of the source is decreased.

#### B. Results of the numerical simulations and analysis

For this purpose, the frequency  $f$  is fixed (125 MHz) while the piston radius  $R_p$  is varied between  $0.5\lambda$  and  $8\lambda$ . Figure 2 represents the isocontours of the modulus of the streaming velocity field (left) and the acoustic velocity field (right), for four values of  $R_p/\lambda$  (1, 3, 5, 8). Note that in all figures,  $r$  and  $z$  denote, respectively, the radial and axial coordinates. One can observe that the streaming velocity (Fig. 2, left) is maximum in the vicinity of the axis in all cases. In addition: (i) The highest velocities are localized in the vicinity of the acoustic source in the case of  $R_p/\lambda = 1$ , and then are shifted away from the source and spread along the axis when  $R_p/\lambda$  increases. (ii) The streaming jet is more and more concentrated around the axis as  $R_p/\lambda$  increases, as

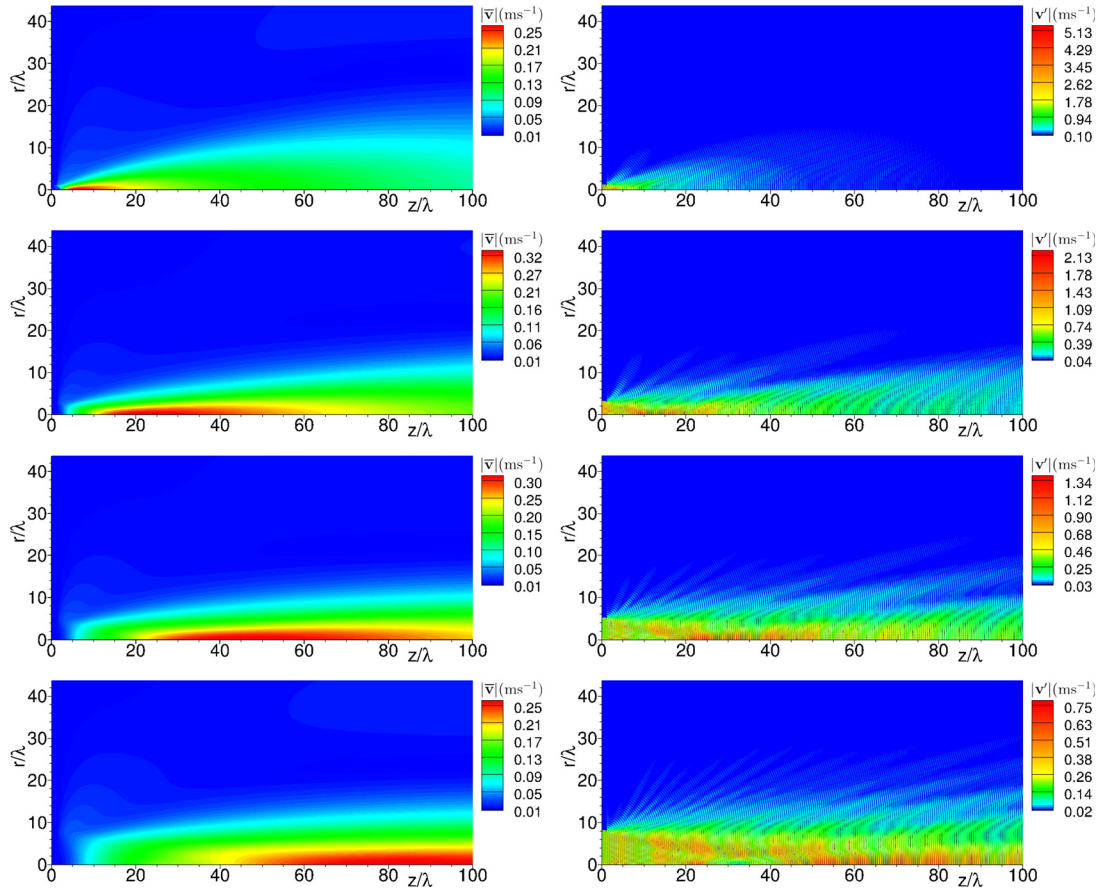


FIG. 2. (Color online) Isolines of the modulus of the mean streaming velocity field  $|\bar{v}|$  (left) and acoustic velocity  $|v'|$  (right). From top to bottom:  $R_p/\lambda = 1, 3, 5, 8; f = 125$  MHz. In these figures,  $r$  and  $z$  denote the radial and axial coordinates, respectively.

can be seen in Fig. 3. Finally, (iii) the maximum streaming velocity ( $|\bar{v}| \approx 0.34$  m/s) is obtained for  $R_p/\lambda \sim 3$ , and decreases for smaller values of  $R_p/\lambda$  (Fig. 4).

All these effects result from an increase in the acoustic diffraction as  $R_p/\lambda$  decreases (Fig. 2, right). Indeed, diffraction (i) leads to the nearly cancellation, at a distance of a few wavelengths (for the smallest aperture) of the acoustic signal and thus of the source term responsible for the jet

generation, (ii) spreads the acoustic signal and thus the streaming source terms laterally, and (iii) prevents the possibility to concentrate the acoustic energy by reducing the transducer dimension to produce high-speed streaming. This cancellation of the streaming source terms at a few wavelengths away from the source for the smallest aperture is

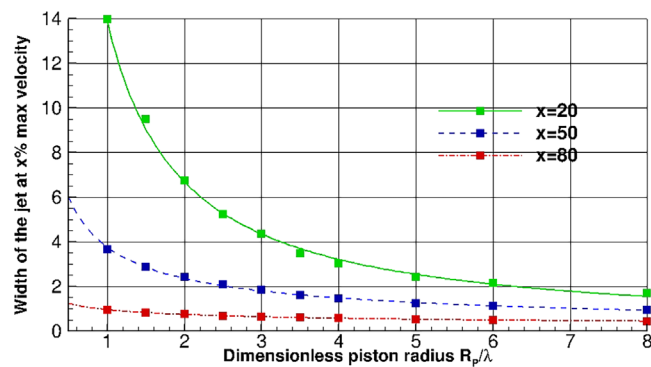


FIG. 3. (Color online) Ratio of the radius of the jet defined as the isocontour corresponding to 20% (green solid line), 50% (blue dashed line), 80% (red dashed dotted line) of the maximum streaming velocity divided by  $R_p/\lambda$ , as a function of  $R_p/\lambda$  at  $f = 125$  MHz. Squares correspond to the numerical simulations. Lines correspond to interpolation of the numerical points.

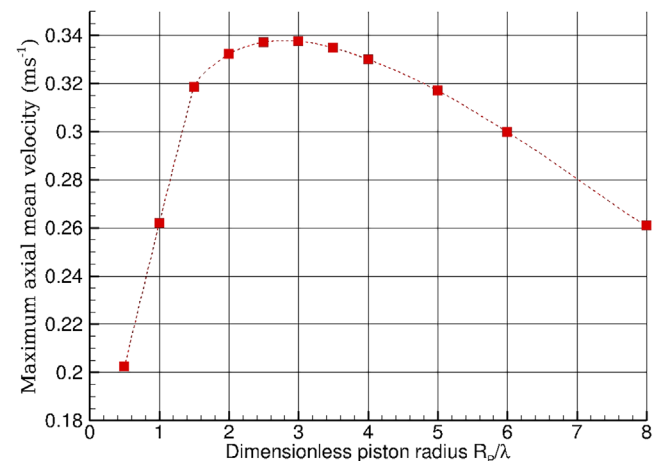


FIG. 4. (Color online) Maximum axial mean velocity as a function of the dimensionless piston radius  $R_p/\lambda; f = 125$  MHz. Red squares correspond to the numerical simulations. Dashed dotted line corresponds to an interpolation of the numerical points.

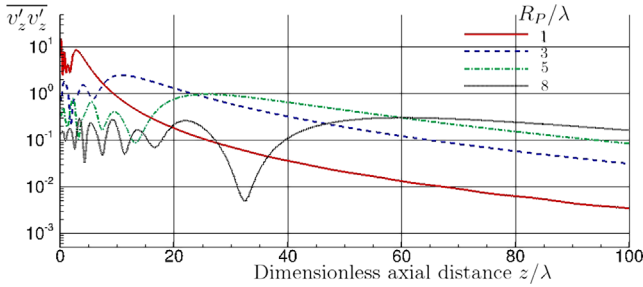


FIG. 5. (Color online) Source term  $\overline{v'_z v'_z}$  along the axis, in log scale, for  $R_p/\lambda = 1, 3, 5, 8; f = 125$  MHz.

clearly visible in Fig. 5, which represents the dominant streaming source term (Moudjed *et al.*, 2014)  $\overline{v'_z v'_z}$ , along the axis, in log coordinates.

To understand the genesis of acoustic streaming in these different configurations, it is also interesting to look at the temporal evolution of the streaming velocity along the axis, for different values of  $R_p/\lambda$ , which is made possible by our direct numerical simulations (Fig. 6; Mm. 1 and Mm. 2). In this figure, all curves are spaced by a constant time interval of 40 000 time periods (corresponding to 0.32 ms). This figure shows that the jet is established in a different way for small and large values of  $R_p/\lambda$ . For small values ( $R_p/\lambda = 1$ ), the maximum velocity is rapidly reached near the acoustic source due to the localization of the source terms, and the velocity field is then transported by advection and/or diffusion. Note that in these simulations, the jet Reynolds number  $Re = \rho UD/\mu$ , with  $\rho$  the density of the fluid at rest,  $U$  the jet characteristic velocity,  $D$  its diameter, and  $\mu$  the dynamic viscosity is relatively constant and on the order of  $Re \sim 30$ , underlying that advection is expected to be dominant over viscous diffusion. For the largest value ( $R_p/\lambda = 8$ ), the velocity increases at approximately the same rate all along the axis, mainly due to the source term that is of the same order

of magnitude everywhere. The advection effect should also be significant in this case, but the two phenomena are in this case entangled.

Mm. 1. Time evolution of the mean velocity  $|\overline{v}|$ .  
 $f = 125$  MHz;  $R_p/\lambda = 1$ .

Mm. 2. Time evolution of the mean velocity  $|\overline{v}|$ .  
 $f = 125$  MHz;  $R_p/\lambda = 8$ .

This section brings the conclusion that the only way to obtain a high-speed localized jet is to increase the frequency to be able to concentrate laterally the streaming source without increasing diffraction effects.

#### IV. FREQUENCY SCALING OF STREAMING JETS

##### A. Problem statement

Following this idea, we will now study the evolution of the acoustic streaming as a function of the actuation frequency. For this purpose, the piston radius is now fixed to  $R_p = 2\lambda$  and the actuation frequency is varied from 37.5 MHz to 3 GHz.

##### B. Results of numerical simulations and analysis

Before delving into the simulations, it is interesting to compare the acoustic wave attenuation length,  $L_a = \rho_0 c_0^3 / 2\pi^2 f^2 (\frac{4}{3}\mu + \mu_B)$ , with the Fresnel length,  $L_f = 2R_p^2/\lambda$ , in the simulated range of parameters (Fig. 7). The attenuation length characterizes the attenuation, while the Fresnel length characterizes the transition between the near field and the far field wherein the acoustic beam is spreading laterally. Figure 7 shows that the attenuation length and the Fresnel length become of the same order of magnitude for frequencies of a few GHz.

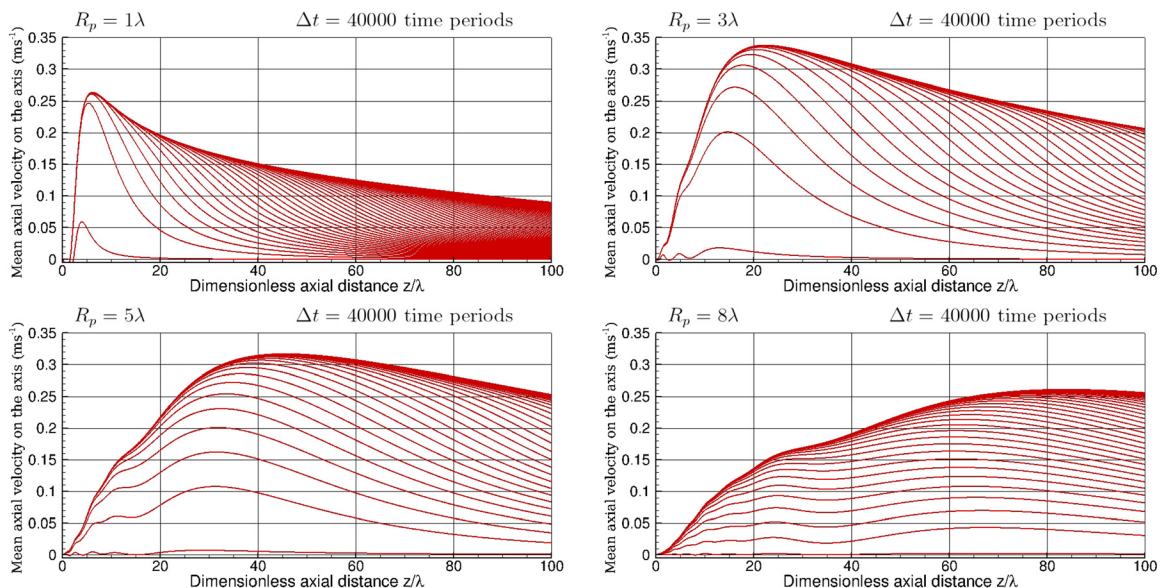


FIG. 6. (Color online) Axial mean velocity along the axis at time intervals  $\Delta t = 40000 T$  ( $T$  is the time period), from left to right and top to bottom:  $R_p/\lambda = 1, 3, 5, 8; f = 125$  MHz.

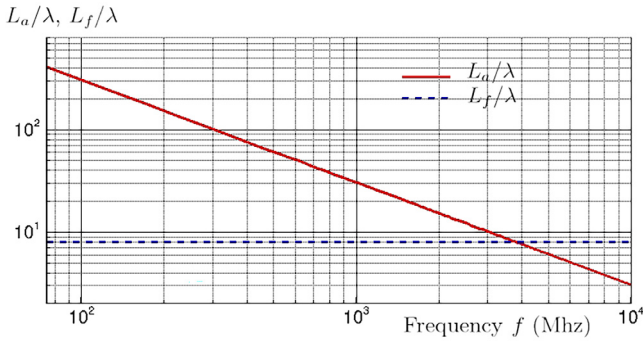


FIG. 7. (Color online) Dimensionless attenuation length  $L_d\lambda$  (red continuous line) and dimensionless Fresnel length  $L_f/\lambda = 2R_p^2/\lambda^2 = 8$  (blue dotted line) as a function of the frequency, in log scale.

The isocontours of the modulus of the streaming velocity field and the acoustic velocity field are represented in Fig. 8 for four values of the frequency (75, 125, 500, and 2000 MHz). This figure shows that the acoustic signal becomes diffracted for axial distances  $z$  exceeding the Fresnel length,  $L_f = 2R_p^2/\lambda$ , i.e., for  $z/\lambda \sim 8$  (since  $R_p/\lambda = 2$ ), hence leading to a local reduction of the streaming source intensity. In addition, the acoustic wave is rapidly attenuated for the highest frequencies leading to highly localized streaming source terms close to the source. The jet structures

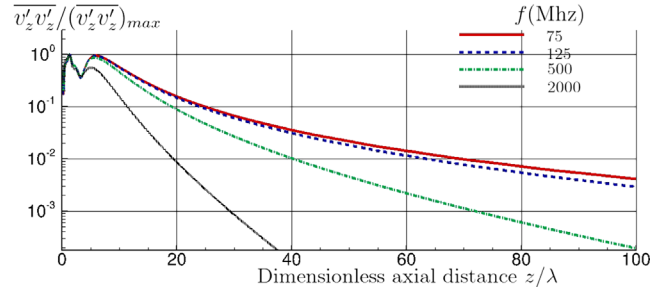


FIG. 9. (Color online) Source term  $\overline{v'_z v'_z}$  along the axis, normalized with the maximum value, for frequencies  $f = 75, 125, 500, 2000$  MHz;  $R_p/\lambda = 2$ .

are modified accordingly with the highest speed in the close vicinity of the piston. The spatial localization of the streaming source can also be seen (i) in Fig. 9, which depicts the dominant streaming source term,  $\overline{v'_z v'_z}$ , in log scale along the central axis and (ii) the temporal evolution of the average streaming velocity on the central axis (Fig. 10). This last figure shows that, while the established flow velocity profiles look relatively similar: (i) The ratio between the maximum and minimum velocity (the latter being obtained at the exit section of the cylinder) increases with the frequency due to the stronger localization of the forcing at high frequency. (ii) The fluid is first accelerated close to the transducer over a distance  $\sim L_a$  and then convected to larger  $z$  at high

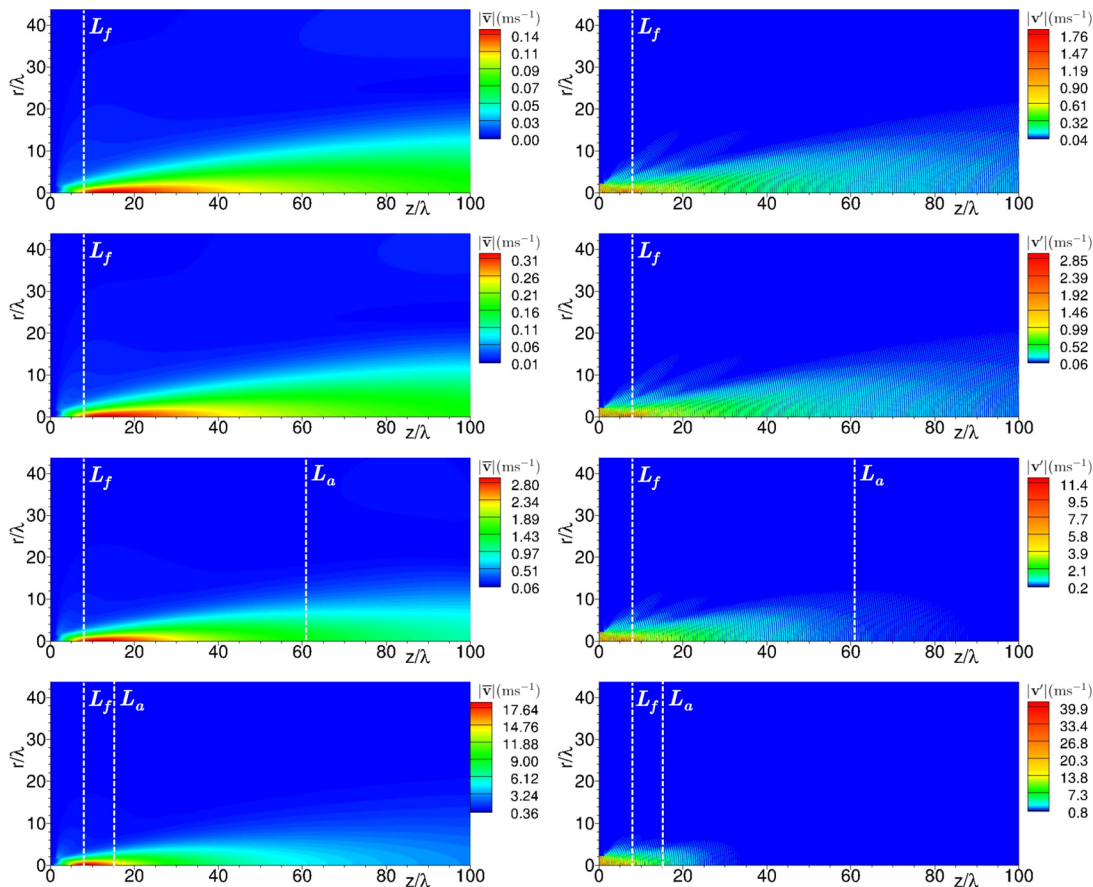


FIG. 8. (Color online) Isolines of modulus of mean velocity field (left) and acoustic velocity (right), from left to right and top to bottom:  $f = 75, 125, 500, 2000$  MHz;  $R_p/\lambda = 2$ .  $L_f$  and  $L_a$  correspond to the Fresnel length and the attenuation length, respectively.

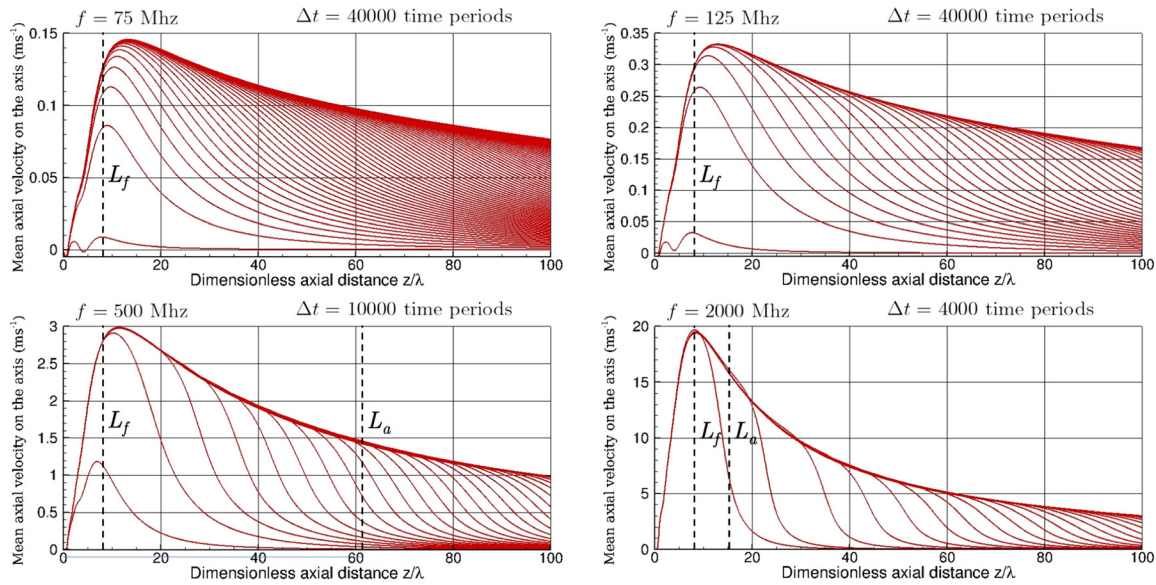


FIG. 10. (Color online) Axial mean velocity along the axis at time intervals  $\Delta t = N_p T$ . From left to right and top to bottom:  $N_p = 40\,000$  for  $f = 75$  and  $125$  Mhz,  $N_p = 10\,000$  for  $f = 500$  Mhz,  $N_p = 4000$  for  $f = 2000$  Mhz;  $R_p/\lambda = 2$ .  $L_f$  and  $L_a$  correspond to the Fresnel length and the attenuation length, respectively.

frequency; while at lower frequencies, the fluid is accelerated simultaneously all along the axis.

The next three figures summarize the interest of high frequency sources to generate high-speed microjets: (i) Fig. 11 shows that the maximum jet speed scales as  $f^{1.52}$  when  $f \leq 1$  GHz, this dependence falling to linear when  $f \geq 1.5$  GHz. This tendency will be explained in the next section with dimensional analysis. This means that increasing the frequency enables to increase the jet speed. (ii) The radius of the jet, defined here as the radius of the isocontour corresponding  $|v|/|v_{max}| = 0.8$  scales as  $f^{-1.2}$  and thus almost as  $\lambda$  for all frequency range (Fig. 12). This can be simply explained by the fact that here the ratio between the source radius and the wavelength  $R_p/\lambda$  is taken as constant; hence, the diffraction is not limiting the scale reduction of the streaming jet, which is therefore proportional to the source radius.

### C. Frequency scaling: A dimensional analysis

Before producing a frequency scale analysis, it is interesting to study the evolution of the Reynolds number  $Re$  introduced previously as a function of the frequency. In the

present simulations,  $\rho \sim 10^3$  and  $\mu \sim 10^{-3}$  are fixed parameters and  $U$  scales as  $f^{1.5}$  below 1 GHz and as  $f$  above (see previous section). Since the diameter of the jet is typically proportional to the wavelength,  $\lambda = c_0/f$ , it means that, below GHz frequencies, the Reynolds number evolves slowly as the square root of the frequency,  $Re \propto \sqrt{f}$ , and is not expected to evolve with frequency in the GHz range. Indeed, based on the simulations (Fig. 8), the diameter of the jet is on the order of  $D = 20\lambda \sim 250 \mu\text{m}$  at 125 MHz and  $D = 5\lambda \sim 7.5 \mu\text{m}$  at 2 GHz, while the velocity is on the order of  $U \sim 0.15 \text{ m s}^{-1}$  at 125 MHz and  $U = 18 \text{ m s}^{-1}$  at 2 GHz, leading to  $Re \sim 40$  at 125 MHz and  $Re \sim 135$  at 2 GHz. These Reynolds number values remain far below the typical threshold value for the transition to turbulent jets of  $Re \sim 2000$ . This analysis indicates that, even if high speeds are reached at high frequency, the jet is not expected to become turbulent. They nevertheless indicate that the convective terms play an important role in this problem.

To obtain a scaling law for the evolution of the jet characteristic speed  $U$  as a function of the frequency, we will start from the integral form of the kinetic energy budget

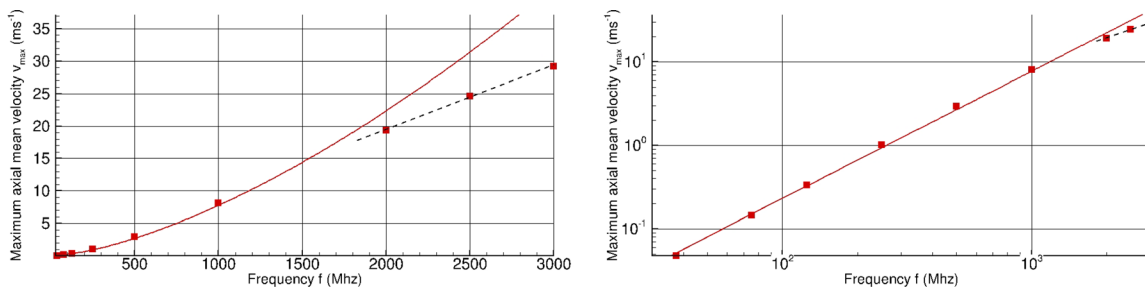


FIG. 11. (Color online) Maximum speed as a function of frequency (in linear scale on the left and log scale on the right). Red squares correspond to the value obtained with the direct numerical simulations. Red continuous line corresponds to the best fit of the numerical points up to 1 GHz with a power law (leading to an exponent of 1.52). Black dotted line corresponds to a linear trend.



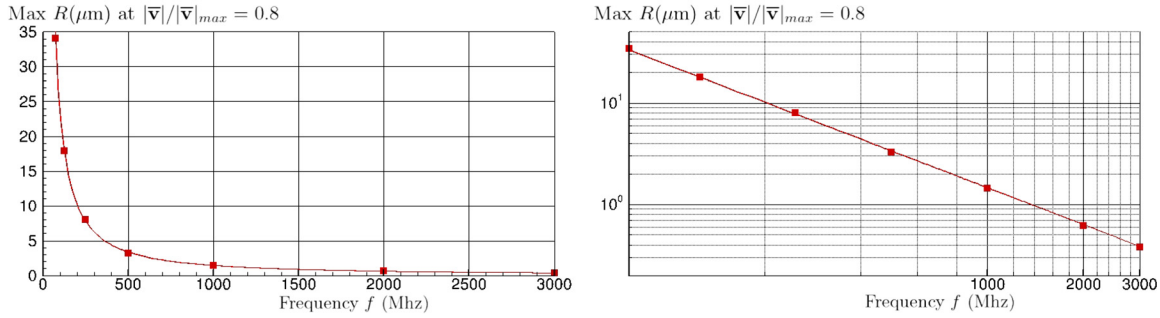


FIG. 12. (Color online) Maximal radius of the jet (in  $\mu\text{m}$ ) at a value of 80% maximum velocity, as a function of  $f$  (in log scale on the right). Red squares correspond to numerical simulations. Red continuous line corresponds to best fit with a power law (coefficient  $-1.2$ ).

equation with a volumetric source term  $\mathbf{f}_s$  corresponding to the streaming source:

$$\begin{aligned} & \iint\int_V \rho_0 \left[ \frac{\partial e_c}{\partial t} + \mathbf{v} \cdot \nabla e_c \right] dV \\ &= \iint\int_V -2\mu \overline{\overline{\mathbf{D}}} : \overline{\overline{\mathbf{D}}} dV + \iint_{\partial V} \overline{\overline{\boldsymbol{\sigma}}}_i \cdot \mathbf{v} \cdot \mathbf{n} dS + \iint\int_V \mathbf{f}_s \cdot \mathbf{v} dV, \end{aligned} \tag{2}$$

with  $e_c = |\mathbf{v}|^2/2$  the kinetic energy density and  $\overline{\overline{\boldsymbol{\sigma}}}_i = -p\mathbf{I} + 2\mu \overline{\overline{\mathbf{D}}}$  the stress tensor in the incompressible regime. Here, we look at the stationary phase so that the time derivative can be neglected. In the fluid acceleration region, the power produced by the streaming force is used to accelerate the fluid and produce kinetic energy. So if we balance the kinetic energy term and streaming source terms in the jet acceleration region,

$$\iint\int_V \rho_0 \mathbf{v} \cdot \nabla e_c dV \sim \iint\int_V \mathbf{f}_s \cdot \mathbf{v} dV,$$

we obtain

$$\frac{\rho_0 U^3}{L} \times \pi R_{jet}^2 L \sim U \int_{z=0}^L f_s(z) dz \times \pi R_{beam}^2,$$

with  $U$  the characteristic velocity,  $L$  a characteristic length associated with the fluid acceleration driven by acoustic streaming,  $z$  the axial coordinate, and  $R_{jet}$  and  $R_{beam}$  the radius of the jet and beams, respectively. From the simulations (Fig. 8), we can see that the radius of the jet is always comparable to the one of the acoustic beam,  $R_{jet} \sim R_{beam}$ , which will be noted  $R$  thereafter. Then following Moudjed *et al.* (2014), the streaming force scales as  $f_s(z) \sim \alpha I_{source} e^{-2z/L_a} / c_0$  in the approximation of an attenuated quasi-plane wave, with  $\alpha = 1/L_a$  the attenuation coefficient. If we introduce the acoustic power radiated by the source  $P_{source} = \pi R_p^2 I_{source}$ ,

$$\rho_0 U^3 \sim \frac{P_{source} \alpha U}{c_0 \pi R_p^2} \int_{z=0}^L e^{-2z/L_a} dz,$$

i.e.,

$$U \sim \left[ \frac{P_{source} \alpha}{\rho_0 c_0 \pi R_p^2} \int_{z=0}^L e^{-2z/L_a} dz \right]^{1/2}.$$

We can note that the scaling law obtained here is similar to the one obtained by Moudjed *et al.* (2014) for near field streaming jets, but here with an integral formulation. Since the streaming force is proportional to the intensity of the beam, fluid acceleration mainly occurs in the region of high beam intensity. As already discussed, the beam intensity decreases due to two phenomena: (i) diffraction and (ii) attenuation. Hence, the characteristic length  $L$  of fluid acceleration corresponds to the minimum of the attenuation length and the Fresnel length:  $L = \min(L_f, L_a)$ . Note that in all the simulations performed at different frequencies in this section,  $L_f \lambda = 2(R_p/\lambda)^2$ , is kept constant:  $L_f \lambda = 8$ , but that the attenuation length decreases as the square of the frequency.

Two asymptotic cases can be distinguished: first, when  $L_f \ll L_a$ ,  $\int_{z=0}^{L=L_f} e^{-2z/L_a} dz \approx L = L_f$  since  $e^{-2z/L_a} \approx 1$ . We hence obtain

$$U \sim \sqrt{\frac{P_{source} \alpha L_f}{\rho_0 c_0 \pi R_p^2}} = \sqrt{\frac{2P_{source} \alpha}{\rho_0 c_0 \pi \lambda}}. \tag{3}$$

Finally,  $P_{source}$ ,  $\rho_0$ , and  $c_0$  are independent of the frequency,  $\alpha$  scales as  $f^2$  and  $\lambda$  scales as  $1/f$ , so that

$$U \propto f^{3/2}.$$

Second, when  $L_f > L_a$ ,  $\int_{z=0}^{L=L_a} e^{-2z/L_a} dz \approx L = L_a$ , leading to

$$U \sim \left[ \frac{P_{source}}{\rho_0 c_0 \pi R_p^2} \right]^{1/2}, \tag{4}$$

since  $\alpha L_a = 1$ .

Since  $R_p^2 \propto 1/f^2$ , we obtain

$$U \propto f.$$

This analysis shows that, in this regime, the jet speed increase as a function of the frequency results primarily from the reduction of the transducer size  $R_p$ .

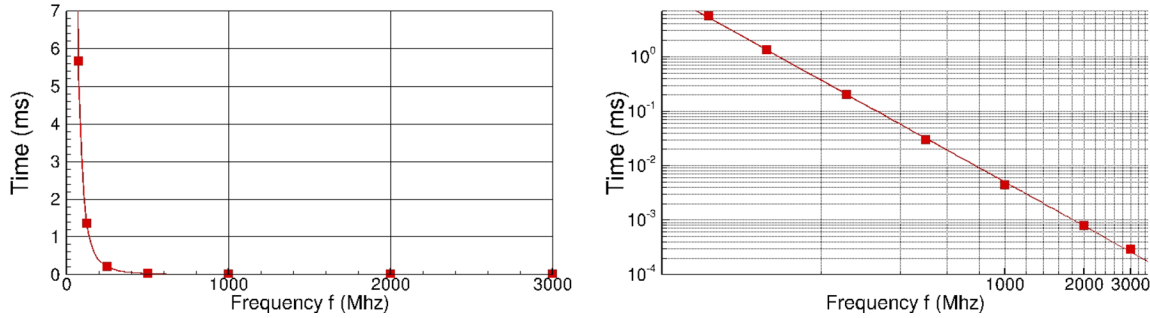


FIG. 13. (Color online) Time necessary to reach the maximum velocity as a function of the frequency, in linear scale (left) and log scale (right). Red squares correspond to numerical simulations. Red continuous line corresponds to best fit with a power law, leading to an exponent  $-2.7$ .

To summarize this section, the scale analysis predicts a transition from a power-law exponent of  $3/2$  to a linear evolution of the jet speed as a function of the frequency when the attenuation length becomes smaller than  $L_f$ . Such transition is expected in the GHz range, which is indeed observed in Fig. 11.

### V. FROM DECA- TO MEGA-G ACCELERATIONS

In this section, we explore an intriguing aspect of GHz streaming that, to the best of our knowledge, has not been previously documented in the literature but holds significant practical relevance for generating ultra-short and powerful jets. This aspect pertains to the remarkable reduction in the time  $\tau_M$  required to reach the maximum jet speed as the frequency increases. As depicted in Fig. 13, our observations indicate that this time exhibits a scaling behavior inversely proportional to the frequency to the power of  $-2.7$ . This results in characteristic times of approximately 6 ms at 75 MHz and merely 1  $\mu$ s at 2 GHz. At the latter frequency, this acceleration corresponds to an order of magnitude of approximately 2 Mega-g. These trends in time reduction with increasing frequency can be understood through scaling analysis in the unsteady case. Following Subsection IV C, we can balance the orders of magnitude of the unsteady term and source terms:

$$\iiint_V \rho_0 \frac{\partial e_c}{\partial t} dV \sim \iiint_V \mathbf{f}_s \cdot \mathbf{v} dV,$$

leading to

$$\frac{\rho_0 U^2}{\tau_M} \pi R^2 L \sim \frac{P_{source} \alpha U}{c_0 \pi R_p^2} \int_{z=0}^L e^{-2z/L_a} dz.$$

Since  $\int_{z=0}^L e^{-2z/L_a} dz \sim L$  (see previous section), we obtain the following expression of the time  $\tau_M$ :

$$\tau_M = \frac{\rho_0 U \pi R_p^2}{\alpha P_{source}}.$$

Since  $R_p^2$  scales as  $1/f^2$ ,  $\alpha$  as  $f^2$ , and  $U$  scales as  $f^{3/2}$  in the weakly attenuated regime and  $f$  in the strongly attenuated regime, this scale analysis predicts that  $\tau_M$  will scale,

respectively, as  $f^{-5/2}$  and  $f^{-3}$  in these two regimes. No clear transitions between the two regimes are seen in Fig. 13, but the power  $-2.7$  obtained from the best fit of the numerical points lies between these two limit values.

### VI. ON THE LIMIT OF CLASSICAL ASYMPTOTIC DEVELOPMENTS

To explore the limits of classical asymptotic developments, it is interesting to compare the maximum streaming axial velocity  $|\bar{v}_{max}|$  to the piston source velocity  $v_p$  and acoustic particular velocity  $|v'|$ .

#### A. Streaming velocity vs piston velocity

Comparison to the piston velocity is provided in Fig. 14. This figure shows that  $|\bar{v}_{max}|/v_p$  scales approximately as the square root of the frequency when  $L_f \ll L_a$  and tends toward a constant when  $L_f > L_a$ . Indeed,  $P_{source} = \overline{p_{source} v_{source}} \times \pi R_p^2$ , where  $p_{source}$  and  $v_{source}$  correspond to the acoustic fluid velocity in the vicinity of the source. Due to the velocity continuity condition on the piston  $v_{source} = v_p$ , and assuming plane wave laws close the piston,  $P_{source} = \rho_0 c_0 v_{source} = \rho_0 c_0 v_p$ , leading to

$$P_{source} = \rho_0 c_0 v_p^2 \pi R_p^2 / 2. \tag{5}$$

Now we can examine the two asymptotic limits. When  $L_f \ll L_a$ , we can combine Eq. (5) with Eq. (3). We obtain

$$\frac{U}{v_p} \sim \sqrt{\alpha L_f},$$

a relation close to the one obtained by Orosco and Friend (2022) in the vicinity of the source, but here under an integral form. Now since  $\alpha \propto f^2$  and  $L_f = 2R_p^2/\lambda \propto 1/f$ , we obtain

$$\boxed{\frac{U}{v_p} \propto \sqrt{f}},$$

which is consistent with the tendency exhibited in Fig. 14 (0.6 power law). When  $L_f > L_a$ , the velocity tends toward a constant limit which is obtained from the combination of Eq. (5) and Eq. (4), i.e.,

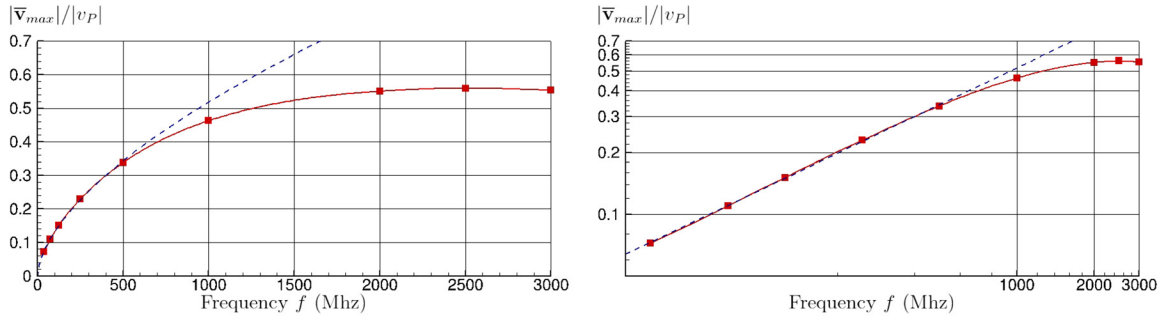


FIG. 14. (Color online) Ratio of the maximum streaming velocity  $|\bar{v}_{max}|$  divided by the acoustic (piston) velocity  $v_p$  as a function of the frequency (in linear scale at the left, and log scale at the right). Red squares corresponds to the numerical simulations. Red continuous line corresponds to an interpolation of the numerical points. Black dotted line corresponds to the best fit of the numerical points up to 500 MHz with a power law (leading to an exponent of 0.6).

$$\frac{U}{v_p} \sim \sqrt{1/2} \approx 0.7.$$

Note that this asymptotic value was also obtained by [Orosco and Friend \(2022\)](#). We see from Fig. 14 that the streaming velocity is indeed saturating toward a value on the order of 0.6. So the scale analysis gives even a quantitative approximation of the asymptotic limit.

### B. Streaming velocity vs acoustic particle velocity

It is now interesting to compare the streaming velocity to the acoustic particular velocity. Figure 15 shows that, at GHz frequencies, the mean velocity can be of the same order as the acoustic particular velocity in the entire region giving birth to acoustic streaming. This figure underlines that classical asymptotic expansion stating that the streaming velocity is small compared to the acoustic velocity is no longer valid at these frequencies.

## VII. DISCUSSION: ON THE FREQUENCY LIMITS OF THIS ANALYSIS

To conclude this article, it is interesting to discuss the frequency limitations of the numerical simulations and

asymptotic analysis presented herein. First, it is important to note that the attenuation of an acoustic wave scales as the frequency square and hence becomes strong in the GHz range. When the attenuation length  $L_a$  becomes commensurable with the wavelength  $\lambda$ , there is no acoustic wave anymore, since it is damped before it can even propagate. In water, this occurs for frequencies on the order of 30 GHz. Second, we assume here an isentropic evolution, which means that thermal dissipation is neglected. This assumption is generally reasonable in liquids since viscous dissipation is dominant. Indeed, asymptotic analysis shows that the ratio between thermal and viscous dissipation scales as  $(\gamma - 1)$  ([Coulouvrat, 1992](#)), with  $\gamma$  the specific heat ratio very close to 1 in liquids. Nevertheless, due to the strong attenuation at GHz frequencies, thermal effects could become significant and lead to some modification of the properties of the liquid (density, viscosity, sound speed), affecting the streaming flow ([Joergensen and Bruus, 2023](#)). These effects will be considered in future work. Finally, we remain here in the approximation of equilibrium thermodynamics and continuum mechanics. Hence, the excitation of vibrational modes of the molecules is not considered. For water, the excitation of molecular vibrations occurs in the THz range.

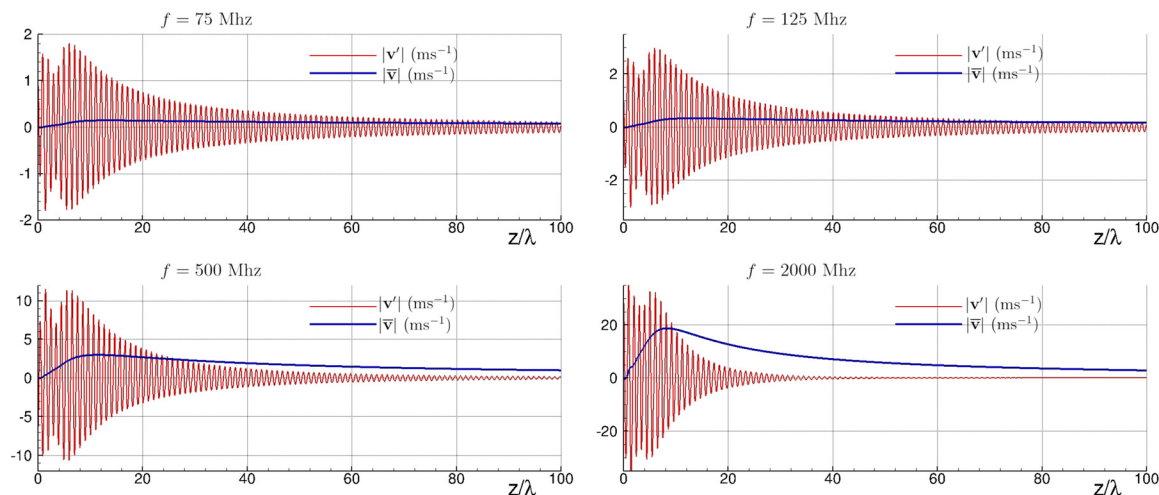


FIG. 15. (Color online) Mean velocity (blue) and acoustic velocity (red) along the axis (in  $\text{ms}^{-1}$ ), from left to right and top to bottom:  $f=75, 125, 500, 2000$  MHz;  $R_p/\lambda=2$ .

## VIII. CONCLUSION

In this paper, we present the first direct numerical simulation of bulk acoustic streaming in a realistic configuration. By coupling these simulations with a scale analysis, we elucidate the scaling law dependency of acoustic streaming on frequency and explain why micro-jets with speeds in meters per second can only be achieved at GHz frequencies. This theoretical investigation also reveals a fascinating aspect of GHz acoustic streaming: achieving such high speeds could take just microseconds, resulting in remarkable acceleration in the Mega-g range. This aspect opens up new possibilities for generating ultra-short, high-speed microjets.

## ACKNOWLEDGMENTS

We acknowledge the support of the ERC Generator and Prematuration project programs funded by ISITE Université Lille Nord-Europe as well as funding from Institut Universitaire de France.

## AUTHOR DECLARATIONS

### Conflict of Interest

The authors report no conflict of interest.

## DATA AVAILABILITY

The data that support the findings of this study are available from the corresponding author upon reasonable request.

Baudoin, M., Gerbedoen, J.-C., Riaud, A., Bou Matar, O., Smagin, N., and Thomas, J.-L. (2019). "Folding a focalized acoustical vortex on a flat holographic transducer: Miniaturized selective acoustical tweezers," *Sci. Adv.* **5**, eaav1967.

Baudoin, M., and Thomas, J.-L. (2020). "Acoustical tweezers for particle and fluid micromanipulation," *Annu. Rev. Fluid Mech.* **52**, 205–234.

Baudoin, M., Thomas, J., Al Sahely, R., Gerbedoen, J., Gong, Z., Sivery, A., Bou Matar, O., Smagin, N., Favreau, P., and Vlandas, A. (2020). "Spatially selective manipulation of cells with single-beam acoustical tweezers," *Nat. Commun.* **11**, 4244.

Chen, S., Wang, Q., Wang, Q., Zhou, J., and Riaud, A. (2023). "Numerical simulation of the radiation force from transient acoustic fields: Application to laser-guided acoustic tweezers," *Phys. Rev. Appl.* **19**(5), 054057.

Collins, D., Devendran, C., Ma, Z., Ng, J. W., Neild, A., and Ai, Y. (2016a). "Acoustic tweezers via sub-time-of-flight regime surface acoustic waves," *Sci. Adv.* **2**(7), e1600089.

Collins, D., Ma, Z., and Ai, Y. (2016b). "Highly localized acoustic streaming and size-selective submicrometer particle concentration using high frequency microscale focused acoustic fields," *Anal. Chem.* **88**, 5513–5522.

Coulouvrat, F. (1992). "On the equations of nonlinear acoustics," *J. Acoustique* **5**, 321–359.

Cui, W., He, M., Yang, Y., Zhang, H., Pang, W., and Duan, X. (2018). "Hypersonic-induced 3D hydrodynamic tweezers for versatile manipulations of micro/nanoscale objects," *Part. Par. Syst. Char.* **35**(8), 1800068.

Cui, W., Mu, L., Duan, X., Pang, W., and Reed, M. A. (2019). "Trapping of sub-100 nm nanoparticles using gigahertz acoustofluidic tweezers for biosensing applications," *Nanoscale* **11**(31), 14625–14634.

Cui, W., Zhang, H., Zhang, H., Yang, Y., He, M., Qu, H., Pang, W., Zhang, D., and Duan, X. (2016). "Localized ultrahigh frequency acoustic fields induced micro-vortices for submillisecond microfluidic mixing," *Appl. Phys. Lett.* **109**(25) 253503.

Daru, V., and Gloerfelt, X. (2007). "Aeroacoustic computations using a high-order shock-capturing scheme," *AIAA J.* **45**(10), 2474–2486.

Daru, V., and Tenaud, C. (2004). "High order one-step monotonicity-preserving schemes for unsteady compressible flow calculations," *J. Comput. Phys.* **193**, 563–594.

Daru, V., and Tenaud, C. (2009). "Numerical simulation of the viscous shock tube problem by using a high resolution monotonicity-preserving scheme," *Comput. Fluids* **38**, 664–676.

Dentry, M., Yeo, L., and Friend, J. (2014). "Frequency effects on the scale and behavior of acoustic streaming," *Phys. Rev. E* **89**(1), 013203.

Ding, X., Lin, S.-C. S., Kiraly, B., Yue, H., Li, S., Chiang, I.-K., Shi, J., Benkovic, S. J., and Huang, T. J. (2012). "On-chip manipulation of single microparticles, cells, and organisms using surface acoustic waves," *Proc. Natl. Acad. Sci. U.S.A.* **109**(28), 11105–11109.

Eisener, J., Lippert, A., Nowak, T., Cairós, C., Reuter, F., and Mettin, R. (2015). "Characterization of acoustic streaming beyond 100 MHz," *Phys. Procedia* **70**, 151–154.

Guo, X., Ma, Z., Goyal, R., Jeong, M., Pang, W., Fischer, P., Duan, X., and Qiu, T. (2020). "Acoustofluidic tweezers for the 3D manipulation of microparticles," in *2020 IEEE International Conference on Robotics and Automation*, pp. 11392–11397.

Gusev, V., and Rudenko, O. (1979). "Nonsteady quasi-one-dimensional acoustic streaming in unbounded volumes with hydrodynamic nonlinearity," *Sov. Phys. Acoust.* **25**, 493–497.

He, M., Zhou, Y., Cui, W., Yang, Y., Zhang, H., Chen, X., Pang, W., and Duan, X. (2018). "An on-demand femtoliter droplet dispensing system based on a gigahertz acoustic resonator," *Lab Chip* **18**(17), 2540–2546.

He, S., Wang, Z., Pang, W., Liu, C., Zhang, M., Yang, Y., Duan, X., and Wang, Y. (2021). "Ultra-rapid modulation of neurite outgrowth in a gigahertz acoustic streaming system," *Lab Chip* **21**(10), 1948–1955.

Hirt, W., Amsden, A. A., and Cook, J. L. (1974). "An arbitrary Lagrangian-Eulerian computing method for all flow speeds," *J. Comput. Phys.* **14**, 227–253.

Joergensen, J., and Bruus, H. (2023). "Theory and modeling of nonperturbative effects in thermoviscous acoustofluidics," *Phys. Rev. E* **107**, 015106.

Kim, Y. C., Blanloeuil, P., Li, D. D., Taylor, R. A., and Barber, T. (2023). "Acoustically driven translation of a single bubble in pulsed traveling ultrasonic waves," *Phys. Fluids* **35**(3) 033315.

Lakin, K., McCarron, K., and Rose, R. (1995). "Solidly mounted resonators and filters," in *IEEE Ultrasonics Symposium Proceedings: An International Symposium*, Vol. 2, pp. 905–908.

Lakin, K. M. (2003). "A review of thin-film resonator technology," *IEEE Microwave* **4**(4), 61–67.

Lighthill, J. (1978). "Acoustic streaming," *J. Sound Vib.* **61**(3), 391–418.

Liu, W., Pan, S., Zhang, H., Tang, Z., Liang, J., Wang, Y., Zhang, M., Hu, X., Pang, W., and Duan, X. (2018). "A universal biomolecular concentrator to enhance biomolecular surface binding based on acoustic NEMS resonator," *ACS Cent. Sci.* **4**(7), 899–908.

Lu, Y., de Vries, W. C., Overeem, N. J., Duan, X., Zhang, H., Zhang, H., Pang, W., Ravoo, B. J., and Huskens, J. (2019). "Controlled and tunable loading and release of vesicles by using gigahertz acoustics," *Angew Chem. Int. Ed. Engl.* **58**(1), 159–163.

Moudjed, B., Botton, V., Henry, D., Ben Hadid, H., and Garandet, J.-P. (2014). "Scaling and dimensional analysis of acoustic streaming jets," *Phys. Fluids* **26**(9) 093602.

Orosco, J., and Friend, J. (2022). "Modeling fast acoustic streaming: Steady-state and transient flow solutions," *Phys. Rev. E* **106**(4), 045101.

Ravi, A., Ruyack, A., Kuo, J., and Lal, A. (2018). "Localized microfluidic mixer using planar Fresnel type GHz ultrasonic transducer," in *IEEE International Ultrasonics Symposium*, pp. 1–4.

Riaud, A., Baudoin, M., Bou Matar, O., Becerra, L., and Thomas, J.-L. (2017a). "Selective manipulation of microscopic particles with precursors swirling Rayleigh waves," *Phys. Rev. Appl.* **7**, 024007.

Riaud, A., Baudoin, M., Matar, O., Thomas, J.-L., and Brunet, P. (2017b). "On the influence of viscosity and caustics on acoustic streaming in sessile droplets: An experimental and a numerical study with a cost-effective method," *J. Fluid Mech.* **821**, 384–420.

Sahely, R. A., Smagin, N., Chutani, R., Matar, O. B., and Baudoin, M. (2022). "Ultra-high frequency vortex-based tweezers for microparticles manipulation with high spatial selectivity and nanonewton forces," [arXiv:2203.05214](https://arxiv.org/abs/2203.05214).

- Shi, X., Bai, Y., Wei, W., and Duan, X. (2022). "3D manipulation and assembly of microstructures using robotic acoustic streaming tweezers," in *IEEE International Ultrasound Symposium*, pp. 1–4.
- Shilton, R., Travagliati, M., Beltram, F., and Cecchini, M. (2014). "Nanoliter-droplet acoustic streaming via ultra high frequency surface acoustic waves," *Adv. Mater.* **26**, 4941–4946.
- Steckel, A., and Bruus, H. (2020). "Numerical simulation of acoustic streaming generated by GHz AlN-thin-film transducers on AlN-SiO<sub>2</sub>-Bragg-reflector substrates," in *Acoustofluidics*, pp. 1–2.
- Stuart, J. (1963). "Laminar boundary layer," in *Unsteady Boundary Layers* (Oxford University Press, Oxford).
- Tran, S., Marmottant, P., and Thibault, P. (2012). "Fast acoustic tweezers for the two-dimensional manipulation of individual particles in microfluidic channels," *Appl. Phys. Lett.* **101**(11) 114103.
- Wang, Q., Riaud, A., Zhou, J., Gong, Z., and Baudoin, M. (2021). "Acoustic radiation force on small spheres due to transient acoustic fields," *Phys. Rev. Appl.* **15**(4), 044034.
- Wei, W., Wang, Y., Wang, Z., and Duan, X. (2023). "Microscale acoustic streaming for biomedical and bioanalytical applications," *Trends Anal. Chem.* **160**, 116958.
- Wu, H., Tang, Z., You, R., Pan, S., Liu, W., Zhang, H., Li, T., Yang, Y., Sun, C., Pang, W., and Duan, X. (2022). "Manipulations of micro/nanoparticles using gigahertz acoustic streaming tweezers," *Nanotechnol. Precis. Eng.* **5**(2) 023001.
- Yang, Y., Zhang, L., Jin, K., He, M., Wei, W., Chen, X., Yang, Q., Wang, Y., Pang, W., Ren, X., and Duan, X. (2022). "Self-adaptive virtual microchannel for continuous enrichment and separation of nanoparticles," *Sci. Adv.* **8**(30), eabn8440.
- Yeo, L., and Friend, J. (2014). "Surface acoustic wave microfluidics," *Annu. Rev. Fluid Mech.* **46**(46), 379–406.
- Zhang, H., Tang, Z., Wang, Z., Pan, S., Han, Z., Sun, C., Zhang, M., Duan, X., and Pang, W. (2018). "Acoustic streaming and microparticle enrichment within a microliter droplet using a Lamb-wave resonator array," *Phys. Rev. Appl.* **9**(6), 064011.
- Zhang, M., He, S., Pang, W., Wei, W., Zhou, F., Wu, X., Qi, H., Duan, X., and Wang, Y. (2022). "On chip manipulation of carbon dots via gigahertz acoustic streaming for enhanced bioimaging and biosensing," *Talanta* **245**, 123462.
- Zuo, C., Van der Spiegel, J., and Piazza, G. (2010). "1.05-GHz CMOS oscillator based on lateral-field-excited piezoelectric AlN contour-mode MEMS resonators," *IEEE Trans. Ultrason. Ferroelectr. Freq. Control* **57**(1), 82–87.